Structural Analysis of "Semisoft" Colloidal Crystals by Confocal Laser Scanning Microscopy

Takashi Morinaga, Kohji Ohno, Yoshinobu Tsujii, and Takeshi Fukuda*

Institute for Chemical Research, Kyoto University, Uji, Kyoto 611-0011, Japan

Received December 25, 2007; Revised Manuscript Received March 6, 2008

ABSTRACT: *Semisoft* colloidal crystals, which are formed by the work of steric or excluded-volume interactions among the *concentrated polymer brushes* (CPBs) afforded on spherical particles, were studied with respect to their crystalline structure as a function of graft chain length, while the graft density was approximately fixed at a high value. Rhodamine-labeled, low-polydispersity silica particles (average diameter 590 nm) were synthesized using the sol−gel chemistry based on the Stöber method and then grafted with a shell of well-defined poly(methyl methacrylate) high-density brush by surface-initiated atom transfer radical polymerization. The internal structure of colloidal crystals formed in a liquid suspension of those hybrid particles was directly (in situ) observed by confocal laser scanning microscopy in fluorescence mode. The crystalline structure was of close-packed type in all cases, and the nearest-neighbor interparticle distance in the crystal increased with increasing graft chain length. The crystals consisted of two-dimensional hexagonal close-packed planes which are stacked in a statistical sequence of hexagonal close-packed (hcp) and face-centered cubic (fcc) lattice arrangements. The probability α of finding a fcc stacking was about 0.59 in a region of relatively short graft chains and substantially equal to 1.0 (perfect fcc) in a region of relatively long graft chains, exhibiting a rather narrow intermediate transition region, where α steeply increased with increasing chain length. This transition of crystalline structure from a nearly random stacking to the fcc arrangement was ascribed to a qualitative change in graft chain conformation and hence interparticle potential curve accompanying the previously noted CPB-to-SDPB (semidilute polymer brush) crossover in the effective graft density of the polymer layer (Ohno et al. *Macromolecules* 2007, *40*, 9143). These results are the first to experimentally show a greater prevalence of fcc stacking as the interaction becomes of longer range. Semisoft colloidal crystals of CPB-afforded hybrid particles can thus cover, by simply changing the graft chain length, a wide range of crystallization concentrations and interparticle potentials between those of typical hard and soft colloidal crystals.

Introduction

Spherical particles suspended in a closed liquid system can organize themselves into a colloidal crystal, even when only repulsive interactions exist between particles (cf. the Kirkwood−Alder transition[1,2]). Typically two types of repulsive potentials have been observed to lead colloidal crystallization. One is the hard-sphere potential, which is steric and short-range in nature, inducing crystallization of rigid uncharged particles (*hard* colloidal crystals).[3−11] The other is the electrostatic potential, which can be of extremely long range depending on the ionic strength of the system, inducing crystallization of charged particles (*soft* colloidal crystals).[12−20]

We recently developed a third type of colloidal crystals, *semisoft* colloidal crystals, in which the driving force of crystallization is the excluded-volume interactions between polymer chains densely grafted on spherical particles.[21,22] This system is distinguished from any of previously observed colloidal crystals or similar ordered assemblies formed by e.g. block copolymers and star-shaped polymers. In fact, colloidal crystals of spherical particles with polymer chains terminally grafted on the surface have been known since early 1970s, and it has been speculated that those graft chains would work as a repulsive interparticle potential, a rather "soft" potential qualitatively analogous to the electrostatic one. However, in all of the previously studied systems of this kind,[3,4,7,8,23] the graft density was so low and, in many cases, the graft chain length was so small that the graft chains simply played the role of stabilizing the particles, having no dominant effect on the interparticle potential, and thus the system essentially showed the characteristics of a hard colloidal crystal. Using surface-initiated atom transfer radical polymerization (ATRP),[24] we succeeded for the first time in preparing silica particles (SiPs) having a shell layer of well-defined polymer chains densely and thickly end-grafted on the particle surface with no aggregation of particles caused and the narrow distribution of particle size maintained throughout the course of preparation.[25] The surface density of the grafted poly(methyl methacrylate) (PMMA) chains reached some 0.7 chains/nm^2, going deeply into the regime of *concentrated polymer brush* (CPB). CPBs had not attracted much attention until recently, when ATRP and other techniques of living radical polymerization (LRP) proved to be capable of routinely providing well-defined CPB samples, with which experiments got started disclosing a number of unique properties of CPBs,[26,27] essentially different from those of less densely grafted surfaces *semidilute polymer brushes* (SDPBs). Important properties of CPBs relevant to colloidal crystallization include the extremely large thickness of swollen CPB layer, almost comparable to the fully stretched length of graft chains,[28,29] and the non-interpenetrating or immiscible property of confronted CPBs even at extremely high compressing pressures.[27] The latter property contrasts to that of confronted SDPBs, which do interpenetrate or mix with each other beyond a critical pressure because of the less extended conformation of SDPB chains. Thus, the brush−brush interaction is suggested to be qualitatively different between CPB and SDPB systems.

A CPB afforded on a spherical surface has the unique feature that the effective surface density of the brush is not constant but varies with varying radial distance from the sphere center. Accordingly, not only the mean thickness of the brush layer but also the radial concentration profile of polymer segments and hence the interparticle potential should be a function not only of the graft density on the core particle surface and core

* To whom correspondence should be addressed. E-mail: fukuda@scl.kyoto-u.ac.jp.

10.1021/ma7028665 CCC: $40.75
Published on Web 04/30/2008

particle size but also of the chain length of graft polymer. When the chain length is small enough, the whole layer of the CPB afforded on a spherical surface would have properties of "CPB", while as the chain length exceeds a crossover value, the outer surface of the brush layer would begin to show properties of "SDPB". In view of the above-noted general properties of CPB and SDPB, this chain-length-dependent structure of the brush layer should be reflected not only on the layer thickness and the critical concentrations of colloidal crystallization but also on the crystal structure itself.

In a previous work,[22] we carried out dynamic light scattering (DLS), in dilute acetone solution, for a series of narrowly distributed silica particles with a diameter of 130 nm afforded with a PMMA CPB. The observed chain length dependence of hydrodynamic thickness h of the brush layer was interpretable by a modified Daoud−Cotton-type scaling theory, disclosing the presence of a crossover chain length of the brush layer from CPB to SDPB regime. Irrespective of graft chain length, more concentrated suspensions of the hybrid particles showed a phase transition from a (disordered) fluid to a fully crystallized system with a narrow fluid/crystal coexisting regime. The critical concentration of crystallization decreased with increasing graft chain length, and the nearest-neighbor interparticle distance D_{dis} in the crystal approached to a micrometer scale as the graft molecular weight reached about 500 000. Good correlation was observed between D_h and D_{dis} such that $D_{dis} = D_h \times (1.15 \pm 0.05)$. A confocal laser scanning microscopic (CLSM) analysis of reflection mode suggested that the structure of the colloidal crystal was not independent of graft chain length but a mixture of hexagonal close-packed (hcp) and face-centered cubic (fcc) lattices with the fraction of hcp lattice likely to increase with decreasing chain length. However, since the resolution of CLSM of reflection mode was not high enough, especially for small particle sizes and short interparticle distances, we could not disclose any more details of the chain length dependence of crystal structure.

In this work, we have carried out a fluorescene-mode CLSM anaylysis with a series of fluorescence-labeled silica−CPB hybrid particles having a larger core diameter (590 nm) and a wider range of PMMA graft chain lengths (from 75 000 to 1 099 000 in weight-average molecular weight, M_w). In the literature, structural analysis of colloidal crystals has been made by scattering methods[6,14–17] and microscopic observations.[10,11,17,18,23,30–32] For samples containing microcrystallites of relatively large size such as colloidal crystals, it is difficult to obtain accurate structural information by scattering methods because the scattering volume is usually too small to contain a statistically sufficient number of crystallites. An excellent work that overcame this difficulty was done by Pusey et al.,[6] who designed a laser light scattering instrument with a 1 cm^3 scattering volume, large enough to obtain statistically accurate data, and successfully determined the structure of a hard colloidal crystal. This method, however, is not easily accessible to all. Microscopic techniques allow direct observation of crystalline structure in real space. However, conventional optical microscopy basically provides precise information only of or near the surface layer of crystallite. When one tries to focus below the surface plane, one will usually have a mixed image of multiple out-of-focus planes. In fact, previous conventional microscopic studies dealt with the observation of only one plane per crystallite.[11,31] Confocal laser scanning microscopy (CLSM), especially that of fluorescence mode,[10,23,30,32] provides a powerful and convenient solution to this difficulty. It gives clear images of not only the surface plane but planes located micrometers below the surface. Three-dimensional (3-D) structure can therefore be observed directly in real space.[10,23,30,32] Although similar experiments with higher resolution could be carried out by transmission electron microtomography, it basically is applicable to dry samples but not to colloidal crystals.[33] Thus, CLSM of fluorescence mode seemed to us to be most promising for our purpose.

Table 1. Characteristics of Rhodamine-Labeled Silica Particles Grafted with Concentrated Poly(methyl methacrylate) Brush[a]

sample code	M_w[b]	M_w/M_n[c]	graft density (chains/nm^2)	ρ (g/cm^3)[d]
R1[e]	75 000	1.32	0.55	1.68
R2	159 000	1.21	0.65	1.51
R3	355 000	1.21	0.71	1.37
R4	620 000	1.25	0.75	1.31
R5[e]	1 099 000	1.40	0.88	1.26

[a] The diameter of the rhodamine-labeled silica particle core was 590 nm. [b] Weight-average molecular weight of poly(methyl methacrylate) (PMMA) grafts. [c] Polydispersity index of PMMA grafts. [d] Calculated value of the overall (average) bulk density of the hybrid particles. [e] The mean diameter and relative standard deviation as observed by TEM were 690 nm and 3.7% for R1 and 1310 nm and 3.9% for R5, respectively (cf. Figure 1).

Experimental Section

Materials. Ethyl 2-bromoisobutyrate (2-(EiB)Br, 98%) and (3-aminopropyl)triethoxysilane (APS, 97%) were purchased from Nacalai Tesque Inc., Osaka, Japan. 4,4′-Dinonyl-2,2′-bipyridine (dNbipy, 97%) and rhodamine B isothiocyanate (RITC) were obtained from Aldrich. Tetraethyl orthosilicate (TEOS) was kindly donated by Chisso Corp., Yokohama, Japan. These reagents were used as received. Methyl methacrylate (MMA, 99%) was obtained from Nacalai Tesque Inc. and purified by passing through a column of activated basic alumina to remove inhibitor. 1,2-Dichloroethane (99%), cholorobenzene (99%), 1,2-dibromoethane (99%), chloroform (99%), and *o*-dichlorobenzene (99%) were used as received from Nacalai Tesque Inc.

Synthesis of Rhodamine-Labeled SiP Grafted with Concentrated PMMA Brush. Following the procedure of van Blaaderen et al.,[34] rhodamine-modified triethoxysilane (APS−RITC) was synthesized by stirring a solution of RITC (56 mg) and APS (45 mg) in dry ethanol (3.7 g) for 24 h in a glovebox purged with argon. To this solution of APS−RITC in ethanol, TEOS (14.6 g) and dry ethanol (21.5 g) were added, and then, this mixture was added dropwise over 1 h into a mixture of ammonia solution (28% aqueous solution, 30.3 g) and ethanol (120 g) under mechanical stirring. Thus, generated silica particles were cleaned by five cycles of centrifugation and dispersion in ethanol to remove residual APS−RITC and TEOS. Finally, an ethanol solution containing 3.9 g of rhodamine-labeled silica particles (RhSiPs) was obtained.

RhSiPs were surface-modified with a triethoxysilane derivative having an atom transfer radical polymerization (ATRP)[24] initiating site and grafted with well-defined PMMA concentrated brushes by surface-initiated ATRP of MMA mediated by a copper complex Cu(I)Cl/dNbipy in the presence of free initiator 2-(EiB)Br, as reported previously.[25] The characteristics of RhSiPs grafted with PMMA brushes (PMMA−RhSiPs) are summarized in Table 1.

Praparation of PMMA−RhSiP Suspensions for Colloidal Crystal Formation. The PMMA−RhSiP hybrid particles were dispersed in a mixed solvent, whose density was slightly (by 0.05 g/cm^3) smaller than the overall (average) density of the PMMA−RhSiPs (see Table 1) and whose refractive index was equal to that of the bulk PMMA ($n = 1.49$). The density matching reduces the effect of gravity, which is essential for the system to achieve a thermodynamic equilibrium, and the adjustment of refractive index provides a clear CLSM image of RhSiP core.[3–5,21,30] The compositions of the mixed solvents are given in Table 2.

Confocal Laser Scanning Microscopic Observations of PMMA−RhSiP Suspensions. A PMMA−RhSiP suspension (ca. 0.5 mL) was put into a glass cell (0.8 cm in diameter and 1.5 cm in height) whose bottom was made of a coverslip and whose top was sealed off after the sample was set. Observation was made on an inverted type CLSM (LSM 5 PASCAL, Carl Zeiss, Germany) with a 543 nm wavelength Ar laser and a 63 × objective (Plan Apochromat, Carl

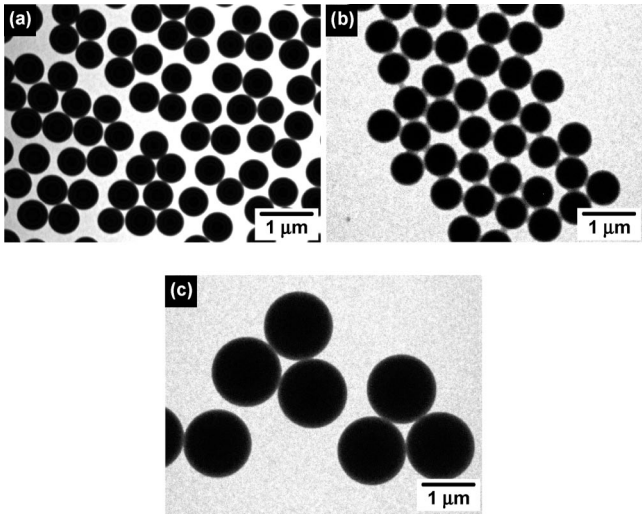

Figure 1. TEM images of (a) rhodamine-labeled silica particles (RhSiPs) and samples (b) R1 and (c) R5.

Table 2. Experimental Conditions and Values of D_{dis} and α

sample[a]	solvent volume ratio[b]	ϕ_m ($\phi_{m,silica}$)[c]	D_{dis}[d] (nm)	α[e]
R1	A/B/C = 47/14/39	0.218 (0.151)	1050	0.59
R2	A/B/C = 49/25/26	0.161 (0.073)	1230	0.60
R3	A/D/E = 36/23/41	0.119 (0.030)	1760	0.58
R4	A/B/E = 57/4/39	0.088 (0.014)	2360	0.76
R5	A/B/E = 52/25/23	0.041 (0.004)	3190	0.89
P3[f]				(35/37)
P5[g]				(26/26)

[a] See Table 1. [b] A: 1,2-dichloroethane; B: chlorobenzene; C: 1,2-dibromoethane; D: chloroform; E: *o*-dichlorobenzene. [c] Melting volume fraction of PMMA−RhSiP hybrid pariticles suspended in the mixed solvent, where CLSM observations were made. Value in parentheses is melting volume fraction of silica core. [d] Nearest-neighbor center-to-center distance of the hybrid particles in the crystal. [e] Probability of fcc (face-centered cubic) stacking. [f] The diameter of the silica core was 130 nm, M_w = 188 000, and the scaled $M_w = M_w \times (590/130) = 853\,000$ (see text). 35 fcc arrangements were found out of 37 of stacking data (the 90% confidence limit of α is 0.85−0.98). [g] The diameter of the silica core was 130 nm, M_w = 518 000, and the scaled $M_w = M_w \times (590/130) = 2\,350\,000$ (see text). 26 fcc arrangements were found out of 26 of stacking data (the 90% confidence limit of α is 0.92−1.00).

Zeiss) in fluorescence mode. The distance of the focal plane from the inside surface of the coverslip was no less than 20 μm. The image analysis software Imaris (Bitplane AG, Zurich, Switzerland) was used to construct a three-dimensional image with CLSM data.

Results and Discussion

Particle Synthesis. Fluorescent dye-labeled silica particles were prepared by the two-step procedure. In the first step, a rhodamine derivative bearing a triethoxysilane moiety (APS−RITC) was synthesized. The second step was the sol−gel reaction of a mixture of TEOS and APS−RITC using the Stöber method[35] to obtain spherical rhodamine-labeled silica particles (RhSiPs). Transmission electron microscopic (TEM) observations revealed that the average diameter of these RhSiPs and its relative standard deviation were 590 nm and 6.8%, respectively (Figure 1). The RhSiPs were functionalized with ATRP initiators and then grafted with a well-defined PMMA high-density brush by surface-initiated ATRP of MMA as reported previously.[25] Thus, we prepared a series of hybrid particles (PMMA−RhSiPs) with a fixed diameter of RhSiP core, nearly the same graft density, and various chain lengths of PMMA grafts (see Table 1). It was difficult to carry out dynamic light scattering measurements with these (R-series of) samples to determine their hydrodynamic diameters and size distributions because of the particles sedimentation (due to their large sizes) and the fluorescence labeling. However, since the method of sample preparation was exactly analogous to the one used in the previous work,[22] we can expect that they should have similar characteristics to those of the previous (P-series of) samples: in particular, we can expect a fairly narrow size distribution also for them. To confirm this, we made TEM observation of two samples (Figure 1) to find their mean diameters and relative standard deviations to be 690 nm and 3.7% for sample R1 and 1310 nm and 3.9% for sample R5, respectively. Incidentally, the diameters of these hybrid particles (in the dry state) calculated with the numerical data in Table 1 and the known bulk density of PMMA were 675 nm for R1 and 1300 nm for R5, in good agreement with the TEM data.

Colloidal Crystallization. By virtue of the density matching, all studied hybrid particles dispersed in the solvent mixture gave, despite their large sizes, an isotropic suspension without showing (positive or negative) sedimentation, allowing us to observe thermodynamically equilibrium or nearly equilibrium phenomena. At a certain narrow range of particle concentrations, where isotropic and crystalline phases coexisted, the suspension exhibited tiny iridescent flecks of crystallites soon after the onset of experiments, and the crystallites very slowly sedimented toward the bottom of the cell, forming, in several days, a sharp boundary between the isotropic and crystalline phases. The volume fraction of crystalline phase increased with increasing particle volume fraction, and the whole suspension was a crystalline phase at the melting volume fraction ϕ_m. This behavior of the R-series samples is essentially similar to what we previously observed for the P-series of samples,[21,22] reminding us of the Kirkwood−Alder transition.[1,2] Values of ϕ_m are listed in Table 2. The table shows that ϕ_m decreases with increasing graft chain length from 0.218 for sample R1 to 0.041 for sample R5, thus covering a wide range of crystallization concentrations between those of typical hard and soft systems.

CLSM Measurement. CLSM observations of the semisoft colloidal crystals in fluorescence mode were carried out for the crystalline phase in the coexisting region of each system (hence the volume fraction ϕ of observation was ϕ_m). Figure 2a shows the three-dimensional (3-D) images of the ordered arrays of RhSiPs formed by sample R4. The crystalline structure can be analyzed by slicing the 3-D image on desired planes. Figure 2b shows the two-dimensional (2-D) close-packed (cp) plane extracted from Figure 2a, corresponding to the (001) plane in the description of Miller index for the *hexagonal system*, in which the cp plane is defined as an $x-y$ plane of a unit lattice. For example, parts c and d of Figure 2 are the (100) and (110) planes, respectively.

Figure 3 collects the CLSM images of the 2-D cp planes of the crystals formed by the hybrid particles with varying graft chain lengths. In all images, the RhSiP cores can be seen as red circles having a mean diameter and diameter distribution in good agreement with those observed by TEM (Figure 1a), regularly dispersed throughout the plane. The PMMA brushes which should be surrounding the RhSiP cores are invisible, as they are not fluorescence-labeled. Noteworthy are not only the high degree of positional order of the RhSiP cores but also the strong dependence of the interparticle distance on the chain length of PMMA grafts. The mean nearest-neighbor center-to-center distance D_{dis} between particles were measured to be 1230, 2360, and 3190 nm in parts a, b, and c of Figure 3, respectively. Values of D_{dis} for all studied systems are listed in Table 2.

The distance D_{dis} can also be estimated from the melting concentration ϕ_m of the crystals, according to the following relation valid for closed-packed structures[22]

$$D_{dis,cal} = 2^{1/6}(V_p/\phi_m)^{1/3} \quad (1)$$

where V_p is the particle volume, in units of nm^3, of PMMA−RhSiP in the dry state (the specific particle volume was approximated by that in the dry state). Figure 4 shows the plot of D_{dis} and $D_{dis,cal}$ as a function of M_w of the graft polymer. A few points may be noteworthy with the figure. The generally good agreement of D_{dis} and $D_{dis,cal}$ will confirm the uniformity of the crystals as well as the consistency of relevant experimental procedures. We previously observed[22] for the P-series of samples that the values of $D_{dis,cal}$ similarly estimated from the ϕ_m data had a good correlation with the hydrodynamic diameters D_h of the hybrid particles determined in dilute suspension, such that $D_{dis,cal}$ ($\approx D_{dis}$) $\approx 1.15D_h$. Although determination of D_h for the present particles was experimentally difficult (see above), we can expect a similar correlation between D_{dis} (or $D_{dis,cal}$) and D_h, and accordingly, the previous discussion about the dependence of brush layer thickness and colloidal crystallization on graft chain length should be valid also for the present system. We will come back to this point later.

Identification of Crystalline Structure. The 2-D cp planes only exist in crystals featuring face-centered cubic (fcc), hexagonal close-packed (hcp), or random hexagonal close-packed (rhcp) structures. The difference between these crystalline structures lies in the sequential stacking of cp planes, which can be made visible by analyzing the plane perpendicular to the cp plane. Of the several crystalline planes perpendicular to the cp plane, the (110) plane most clearly exhibits the difference between fcc and hcp stackings.[11] Using this methodology and the conventional microscopy technique, the crystalline structure of hard colloidal crystal was determined to be of rhcp type. This analysis required a very strict adjustment of the microscope focal plane to the (110) plane of the microcrystallite to be studied. However, in the CLSM analysis combined with the image analysis software Imaris used here, the (110) crystalline planes can be extracted from any microcrystallites regardless of their orientation, and in this regard, it is a much more powerful and versatile method than the one using conventional microscopy.

Figure 5 shows an example of the CLSM image of the (110) crystalline plane (sample R4). As demonstrated in Figure 5b, the fcc stacking is characterized by a linear arrangement of three consecutive spheres in the (110) plane, and the hcp stacking is given by their zigzag arrangement, and therefore these two stacking modes are easily distinguished in the image of the (110) plane. The stacking probability α, i.e., the number fraction of fcc stackings, is given by

$$\alpha = N_{fcc}/(N_{fcc} + N_{hcp}) \quad (2)$$

where N_{fcc} and N_{hcp} are the numbers of fcc and hcp stackings. Hence, $\alpha = 0$, 0.5, and 1 represent (perfect) hcp, rhcp, and (perfect) fcc structures, respectively. To obtain sufficient statistics, we collected, for each sample, about 100 images of (110) planes randomly sampled at different positions of the crystalline phase, each image showing the side view of about a dozen of successive cp planes and hence giving about 10 of stacking data, and thus we studied a total of about 1000 cp planes with their (110) stacking modes ($N_{fcc} + N_{hcp} \approx 1000$).

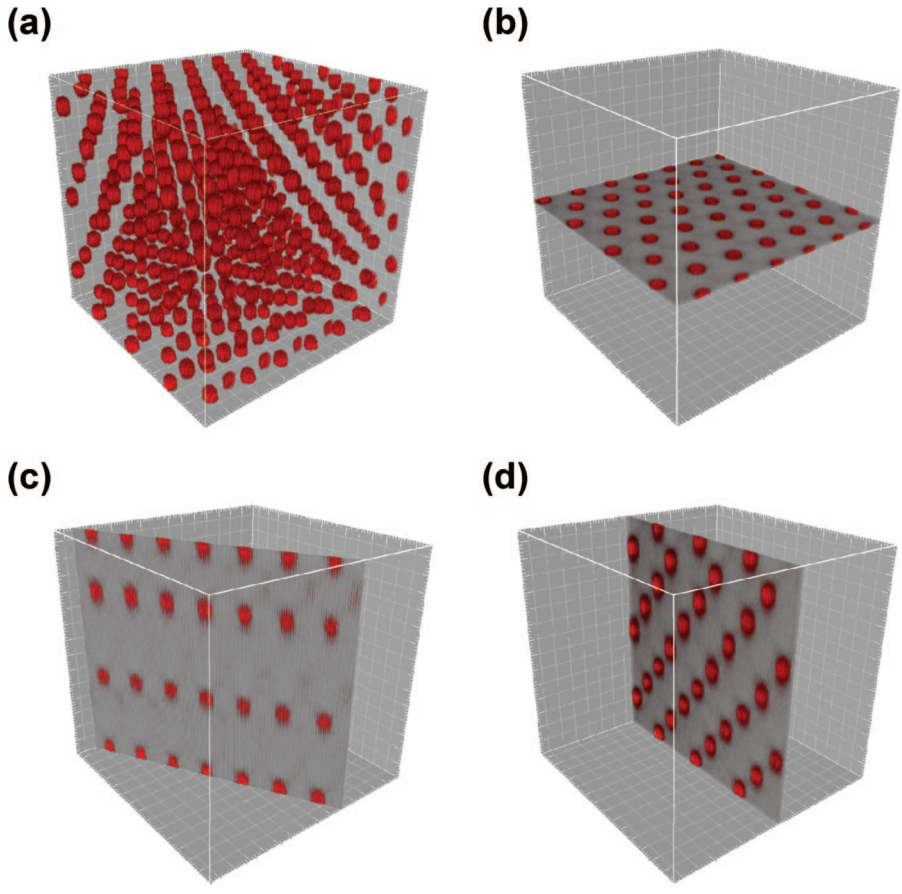

Figure 2. Confocal laser scanning microscopy (CLSM) images of the colloidal crystal formed by rhodamine-labeled silica particles (RhSiPs) grafted with poly(methyl methacrylate) (PMMA) concentrated brush (PMMA−RhSiPs) (sample R4, Table 1). The diameter of RhSiP core is 590 nm, and the weight-average molecular weight of the PMMA grafts is 620 000. Part a shows a three-dimensional image for a part of a microcrystallite. Parts b, c, and d show the images of the (001), (100), and (110) planes, respectively, extracted from (a) by the image analysis software Imaris. Note that these planes are indexed according to the Miller description for the hexagonal system, in which the two-dimensional close-packed plane (001) is defined as an $x-y$ plane of a unit lattice.

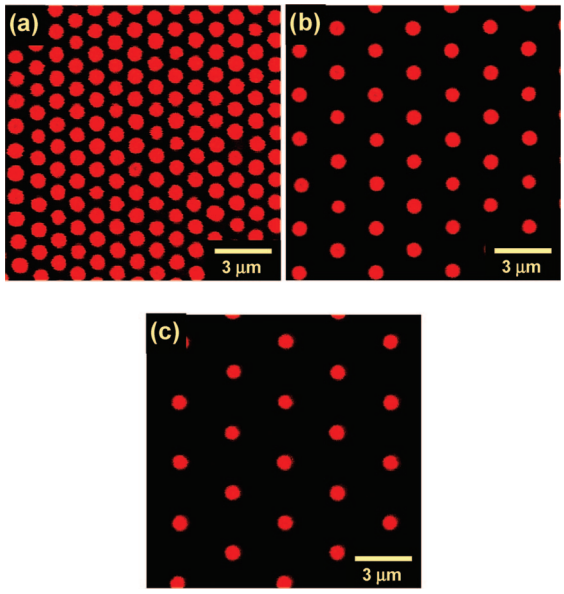

Figure 3. CLSM images of the (001) plane (two-dimensional close-packed plane) of the colloidal crystals formed by PMMA−RhSiP hybrid particles. The weight-average molecular weights of the PMMA grafts are (a) 159 000, (b) 620 000, and (c) 1 099 000. The mean nearest-neighbor center-to-center distances in the images measure (a) 1230, (b) 2360, and (c) 3190 nm. For other details, see Figure 2.

To supplement these data, we also examined the colloidal crystals formed by the P-series of samples which had a SiP diameter of 130 nm and PMMA M_w of 188 000 and 518 000 (samples P3 and P5, respectively, in ref 22). As they were not fluorescence-labeled, we used the laborious and time-consuming reflection mode of CLSM to successfully obtain 37 and 26 of (110) stacking data for P3 and P5, respectively. Since the graft densities of P-series of samples were similar to those of R-series of samples, and since the static or structural properties of such hybrid particles with the same graft density may be reasonably assumed to be scaled or normalized by the ratio of graft chain length to core diameter,[22] the data for P-series of samples with their molecular weights multiplied by the ratio of core diameters (590/130) may be compared with those for R-series of samples. The scaled molecular weights of samples P3 and P5 and their mean values of α and their error ranges are given in Table 2 and its caption, along with the data for R-series of samples.

In Figure 6, α is plotted as a function of logarithm of M_w (or scaled M_w for P-series of samples) of the PMMA grafts. The figure suggests the existence of three regions. In the first region of relatively small chain lengths, α is nearly constant and equal to about 0.59. Namely, in this region, fcc and hcp structures coexist in nearly equal proportion, similar to the rhcp structure in which $\alpha = 0.5$. In the second "transition" region of intermediate chain lengths, α increases rather sharply and approaches 1 with increasing M_w. In the third region of large chain lengths, α is constant and equal to 1.0, i.e., perfect fcc. Because of the lack of sufficient statistics for the sample with the largest M_w (sample P5), we are still unable to experimentally confirm that α is 1.0 for this sample, but the observed trend strongly suggests that $\alpha = 1$ in the third region of larger chain lengths.

The observed chain length dependence of α seems to go in parallel with the chain length dependence of brush layer thickness or graft chain conformation. In the previous work with the P-series of samples,[22] we showed that in a region of small graft chain lengths the whole graft layer is in a CPB (concentrated polymer brush) regime in which the excluded-volume effect is unimportant, while in a region of large chain lengths,

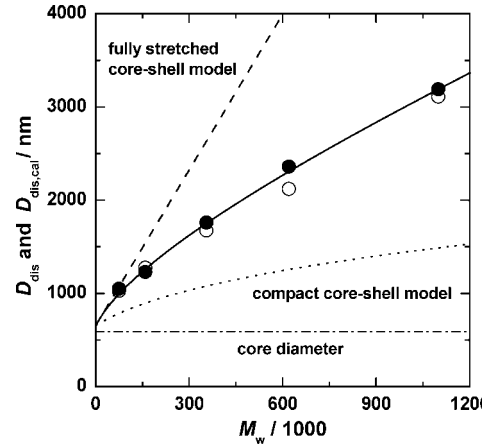

Figure 4. Plot of nearest-neighbor center-to-center distance D_{dis} between particles at the melting concentration of the colloidal crystal as a function of the weight-average molecular weight M_w of PMMA grafts. D_{dis} and (●): observed by CLSM (cf. Figure 3); $D_{dis,cal}$ and (○): calculated with the melting concentration of the crystal (see text and Table 2). The diameter of SiP core is 590 nm. The broken and dotted lines represent the diameters of the fully stretched and compact core−shell models, respectively (see text).

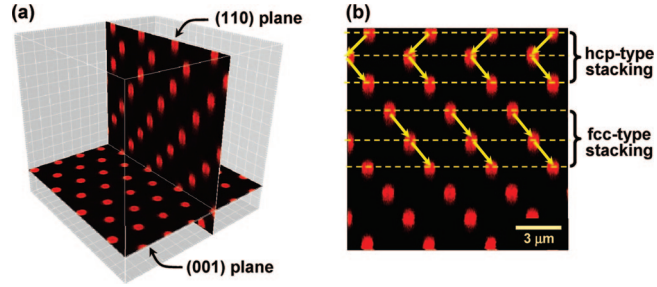

Figure 5. CLSM images of the (001) and (110) crystalline planes of a colloidal crystal (sample R4). Part a shows the spatial relation between the (001) and (110) planes, and part b demonstrates the difference of hcp and fcc stackings appearing in the (110) plane. For other details, see Figure 2 and text.

the brush layer is divided into two regimes by a characteristic radius r_c. In the inside of this radius ($r < r_c$), the brush layer is in a CPB regime, and in the outside of it ($r > r_c$), it is in a SDPB (semidilute polymer brush) regime, where the excluded-volume effect is important. Therefore, the chain conformation and the interparticle potential curve of hybrid particles with short grafts should be very different from those of hybrid particles with long grafts. According to the previous analysis of the hydrodynamic thickness of brush layers, sample P2 with $M_w = 1.26 \times 10^5$ was closely situated on the CPB−SDPB boundary (see Figure 3 in ref 22). In fact, Figure 6 seems to be roughly dividable into CPB and SDPB regimes by the vertical straight line corresponding to this chain length (the scaled $M_w = 5.7 \times 10^5$). In more detail, sample P3 ($M_w = 1.88 \times 10^5$: the scaled $M_w = 8.5 \times 10^5$) was situated just above this boundary of CPB and SDPB regimes. Namely, while the most part of the graft layer of this sample was in a CPB regime, the outermost surface of it was likely in a SDPB regime. Although this was reflected only slightly in the hydrodynamic thickness of the brush layer (cf. Figure 3 in ref 22), even such a small and local change had a large effect on interparticle potential, hence on crystalline structure, as the steep increase in α of this sample showed. Figure 6 shows that sample P3, as well as samples R4 and R5, whose graft chain lengths are similar, have large values of α, forming the "transition" region.

As noted above, our system with graft chains in the CPB regime (or relatively short graft chains) behaved like a hard-

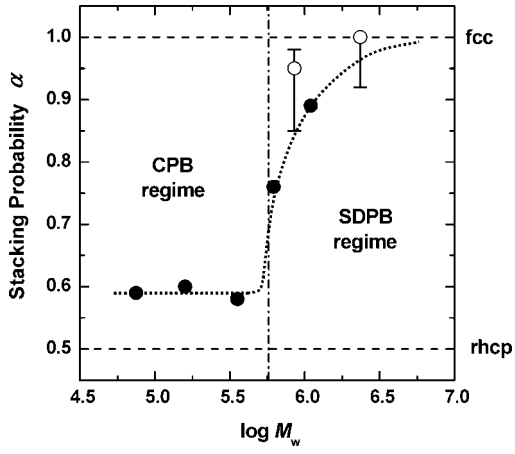

Figure 6. Plot of stacking probability α vs logarithm of weight-average molecular weight M_w of PMMA grafts: (●) observed for R-series of samples by CLMS in fluorescence mode; (○) observed for P-series of samples by CLSM in reflection mode, the vertical line segments showing 90% confidence limits (see Table 2 and text). The 90% confidence limits for R-series of samples are smaller than the diameter of the filled circles. The vertical dot-dash line shows the approximate crossover between CPB and SDPB regimes estimated from the chain length dependence of the hydrodynamic diameter of the P-series of samples (see text and ref 22).

sphere system. This is understandable, since chains in CPB regime are highly extended. They give a large hydrodynamic diameter, even comparable to the dimension of the fully stretched model,[21,36] which consists of a silica core and a PMMA shell whose size is equal to that of the PMMA chains radially stretched in all-trans conformation (cf. Figure 4). As already noted, the crystallization concentrations of our semisoft systems with short (as well as long) graft chains were closely approximated by that of the hard-sphere system having an equivalent hydrodynamic diameter. This along with the mentioned fact that confronted CPBs never interpenetrate or mix with each other (see Introduction) suggests that the interparticle potential between CPB-grafted particles is short-ranged and closely like that between hard spheres, even though the volume fractions of crystallization in the semisoft systems are generally much smaller (cf. Table 2) than that of the hard-sphere system in which $\phi_m = 0.55$. At this stage, we get involved in the controversy regarding the structure of the hard-sphere system.[37] The fcc structure is favored by the theory,[37] but earlier experiments[6,9,10,38,39] indicated a structure close to rhcp. Our result for those samples that are considered to be in the CPB regime indicated that α is about 0.59 with no clear chain length dependence in this region. This will vote for the *experimental favor* of rhcp in hard or quasi-hard systems.

However, our result also indicated that α increased rather sharply as the chain length increased beyond a critical value and approached 1 for the perfect fcc. We explain this dependence of α on graft chain length in terms of the qualitative change in interparticle potential accompanied by the CPB to SDPB crossover. Systems with long graft chains will be characterized by the rather "soft" interparticle potential of SDPBs: as noted above, the crystallization concentrations of SDPB systems are also approximated by that of the hard-sphere system with an equivalent hydrodynamic diameter. Since the hydrodynamic diameter is determined by the average dimension of graft chains and since graft chains in a SDPB system are less extended on average and can take numerous conformations of differing degrees of chain extension, the interparticle potential between SDPB systems should be, unlike that between CPB systems, necessarily of long-range nature.

All these observations and discussion suggest that fcc might be a thermodynamically stable phase in hard as well as semisoft systems. However, during the crystallization process, some hcp arrangements might be frozen in irreversibly. This nonequilibrium process will be more likely to happen for systems with a shorter range of interparticle potential like those of the hard-sphere and CPB systems. The entropy difference between fcc and hcp phases theoretically deduced[37] may be too small to realize an equilibrium system in usual experimental conditions. On the other hand, as the interparticle potential range becomes longer, not only the nearest-neighbor but also the second-nearest (and higher-order) interactions can play a role in crystallization, giving much larger energetic and entropic differences between fcc and hcp phases. Therefore, nonequilibrium processes will be less likely to occur in systems with a longer range of interparticle potential.

Ordering of particle-like polymeric architectures such as star-shaped polymers and block copolymer micelles in solution has been found by both experiment and computer simulation.[40–43] In some cases, structural transformation from fcc to bcc lattice occurred as the interparticle potential became softer.[41,42] In view of these results, our semisoft systems may, in the limit of large chain length relative to core diameter, exhibit a fcc to bcc transition. Thus, we may be able to cover the whole range of possible crystalline structures including rhcp, fcc, and bcc structures with a single CPB−core particle system by simply changing the graft chain length. This remains to be studied as a future target.

Conclusions

The internal structure of the colloidal crystals formed in a liquid suspension of concentrated PMMA brush−SiP hybrid particles was directly observed by CLSM in fluorescence mode (or reflection mode, for some nonlabeled samples). The crystalline structure was of close-packed type in all cases, and the nearest-neighbor interparticle distance in the crystal increased with increasing graft chain length. The crystals consisted of two-dimensional hexagonal close-packed planes which are stacked in a statistical sequence of hcp and fcc arrangements. The probability α of finding a fcc stacking was about 0.59 in a region of relatively short graft chains and substantially equal to 1.0 (perfect fcc) in a region of relatively long graft chains, exhibiting a rather narrow intermediate transition region, where α steeply increased with increasing chain length. This transition of crystalline structure from a nearly random stacking to an fcc arrangement was ascribed to a qualitative change in graft chain conformation and hence interparticle potential curve accompanying the CPB-to-SDPB crossover of the effective graft density. These results are the first to experimentally show a greater prevalence of fcc stacking as the interaction becomes of longer range. Thus, semisoft colloidal crystals of CPB-afforded hybrid particles possibly cover, by simply changing the graft chain length, a wide range of crystallization concentrations and interparticle potentials between those of typical hard and soft colloidal crystals.

Acknowledgment. This work was supported in part by a Grant-in-Aid for Scientific Research (Grant-in-Aid 17002007 and 17685010) from the Ministry of Education, Culture, Sports, Science, and Technology, Japan, and by Industrial Technology Research Grant Program in 2004 from the New Energy and Industrial Technology Development Organization (NEDO) of Japan. We thank Chisso Corp. for their kind donation of TEOS.

References and Notes

(1) Alder, B. J.; Hoover, W. G.; Young, D. A. *J. Chem. Phys.* **1968**, *49*, 3688–3696.
(2) Hoover, W. G.; Ree, F. H. *J. Chem. Phys.* **1968**, *49*, 3609–3617.
(3) Kegel, W. K.; van Blaaderen, A. *Science* **2000**, *287*, 290–293.

(4) Pusey, P. N.; van Megen, W. *Nature (London)* **1986**, *320*, 340–342.
(5) van Megen, W.; Underwood, S. M. *Nature (London)* **1993**, *362*, 616–618.
(6) Pusey, P. N.; van Megen, W.; Bartlett, P.; Ackerson, B. J. *Phys. Rev. Lett.* **1989**, *63*, 2753–2756.
(7) Kose, A.; Hachisu, S. *J. Colloid Interface Sci.* **1974**, *46*, 460–469.
(8) Cheng, Z.; Russel, W. B.; Chaikin, P. M. *Nature (London)* **1999**, *401*, 893–895.
(9) Zhu, J.; Li, M.; Rogers, R.; Meyer, W.; Ottewill, R. H.; Russel, W. B.; Chaikin, P. M. *Nature (London)* **1997**, *387*, 883–885.
(10) Verhaegh, N. A. M.; van Duijneveldt, J. S.; van Blaaderen, A.; Lekkerkerker, H. N. W. *J. Chem. Phys.* **1995**, *102*, 1416–1421.
(11) (a) Elliot, M. S.; Bristol, B. T. F.; Poon, W. C. K. *Physica A* **1997**, *235*, 216–223. (b) Elliot, M. S.; Poon, W. C. K. *Adv. Colloid Interface Sci.* **2001**, *92*, 133–194.
(12) Hachisu, S.; Kobayashi, Y.; Kose, A. *J. Colloid Interface Sci.* **1973**, *42*, 342–348.
(13) Hachisu, S.; Takano, K. *Adv. Colloid Interface Sci.* **1982**, *16*, 233–252.
(14) Sogami, I. S.; Yoshiyama, T. *Phase Transitions* **1990**, *21*, 171–182.
(15) Williams, R.; Crandall, R. S. *Phys. Lett.* **1974**, *48A*, 225–226.
(16) Clark, N. A.; Hurd, A. J.; Ackerson, B. J. *Nature (London)* **1979**, *281*, 57–60.
(17) Yoshida, H.; Yamanaka, J.; Koga, T.; Ise, N.; Hashimoto, T. *Langmuir* **1998**, *14*, 569–574.
(18) Yoshida, H.; Ito, K.; Ise, N. *Phys. Rev. B* **1991**, *44*, 435–438.
(19) Hiltner, P. A.; Krieger, I. M. *J. Phys. Chem.* **1969**, *73*, 2386–2389.
(20) Okubo, T. *Prog. Polym. Sci.* **1993**, *18*, 481–517.
(21) Ohno, K.; Morinaga, T.; Takeno, S.; Tsujii, Y.; Fukuda, T. *Macromolecules* **2006**, *39*, 1245–1249.
(22) Ohno, K.; Morinaga, T.; Takeno, S.; Tsujii, Y.; Fukuda, T. *Macromolecules* **2007**, *40*, 9143–9150.
(23) Gasser, U.; Weeks, E. R.; Schofield, A.; Pusey, P. N.; Weitz, D. A. *Science* **2001**, *292*, 258–262.
(24) (a) Ejaz, M.; Yamamoto, S.; Ohno, K.; Tsujii, Y.; Fukuda, T. *Macromolecules* **1998**, *31*, 5934–5936. (b) Husseman, M.; Malmström, E. E.; McNamara, M.; Mate, M.; Mecerreyes, D.; Benoit, D. G.; Hedrick, J. L.; Mansky, P.; Huang, E.; Russell, T. P.; Hawker, C. J. *Macromolecules* **1999**, *32*, 1424–1431. (c) Matyjaszewski, K.; Miller, P. J.; Shukla, N.; Immaraporn, B.; Gelman, A.; Luokala, B. B.; Siclovan, T. M.; Kickelbick, G.; Vallant, T.; Hoffmann, H.; Pakula, T. *Macromolecules* **1999**, *32*, 8716–8724. (d) Jeyaprakash, J. D.; Samuel, S.; Dhamodharan, R.; Rühe, J. *Macromol. Rapid Commun.* **2002**, *23*, 277–281. (e) Mori, H.; Boker, A.; Krausch, G.; Müller, A. H. E. *Macromolecules* **2001**, *34*, 6871–6882. (f) Kim, J.-B.; Bruening, M. L.; Baker, G. L. *J. Am. Chem. Soc.* **2000**, *122*, 7616–7617. (g) Sedjo, R. A.; Mirous, B. K.; Brittain, W. J. *Macromolecules* **2000**, *33*, 1492–1493. (h) von Werne, T.; Patten, T. E. *J. Am. Chem. Soc.* **1999**, *121*, 7409–7410. (i) Perruchot, C.; Khan, M. A.; Kamitsi, A.; Armes, S. P.; von Werne, T.; Patten, T. E. *Langmuir* **2001**, *17*, 4479–4481. (j) Huang, X.; Wirth, M. J. *Anal. Chem.* **1997**, *69*, 4577–4580. (k) Jones, D. M.; Brown, A. A.; Huck, W. T. S. *Langmuir* **2002**, *18*, 1265–1269.
(25) Ohno, K.; Morinaga, T.; Koh, K.; Tsujii, Y.; Fukuda, T. *Macromolecules* **2005**, *38*, 2137–2142.
(26) Tsujii, Y.; Ohno, K.; Yamamoto, S.; Goto, A.; Fukuda, T. *Adv. Polym. Sci.* **2006**, *197*, 1–45.
(27) Fukuda, T.; Tsujii, Y.; Ohno, K. *Macromolecular Engineering. Precise Synthesis, Materials Properties, Applications*; Matjaszewski, K., Gnanou, Y., Leibler, L., Eds.; Wiley-VCH: Weinheim, 2007; pp 1137−1178.
(28) Yamamoto, S.; Ejaz, M.; Tsujii, Y.; Matsumoto, M.; Fukuda, T. *Macromolecules* **2000**, *33*, 5602–5607.
(29) Yamamoto, S.; Ejaz., M.; Tsujii, Y.; Fukuda, T. *Macromolecules* **2000**, *33*, 5608–5612.
(30) Yethiraj, A.; van Blaaderen, A. *Nature (London)* **2003**, *421*, 513–517.
(31) Kose, A.; Ozaki, M.; Takano, K.; Kobayashi, Y.; Hachisu, S. *J. Colloid Interface Sci.* **1973**, *44*, 330–338.
(32) Weeks, E. R.; Crocker, J. C.; Levitt, A. C.; Schofield, A.; Weitz, D. A. *Science* **2000**, *287*, 627–631.
(33) Schneider, G. J.; Fink, S. A.; Rachel, R.; Göritz, D. *Kaustch. Gummi Kunstst.* **2005**, *58*, 461–463.
(34) Verhaegh, N. A. M.; van Blaaderen, A. *Langmuir* **1994**, *10*, 1427–1438.
(35) Stöber, W.; Fink, A.; Bohn, A. *J. Colloid Interface Sci.* **1968**, *26*, 62–69.
(36) Ohno, K.; Koh, K.; Tsujii, Y.; Fukuda, T. *Angew. Chem., Int. Ed.* **2003**, *42*, 2751–2754.
(37) Woodcock, L. V. *Nature (London)* **1997**, *385*, 141–143.
(38) Frenkel, D.; Ladd, A. J. C. *J. Chem. Phys.* **1984**, *81*, 3188–3193.
(39) Bolhuis, P. G.; Frenkel, D.; Mau, S.-C.; Huse, D. A. *Nature (London)* **1997**, *385*, 235–237.
(40) Witten, T. A.; Pincus, P. A.; Cates, M. E. *Europhys. Lett.* **1986**, *2*, 137–140.
(41) Willner, L.; Jucknischke, O.; Richter, D.; Farago, B.; Fetters, L. J.; Huang, J. S. *Europhys. Lett.* **1992**, *19*, 297–303.
(42) (a) McCornell, G. A.; Gast, A. P.; Huang, J. S.; Smith, S. D. *Phys. Rev. Lett.* **1993**, *71*, 2102–2105. (b) McCornell,; G, A.; Gast, A. P. *Macromolecules* **1997**, *30*, 435–444.
(43) Watzlawek, M.; Likos, C. N.; Löwen, H. *Phys. Rev. Lett.* **1999**, *82*, 5289–5292.

MA7028665